STABILIZATION MECHANISMS OF SWIRLING PREMIXED FLAMES WITH AN AXIAL-PLUS-TANGENTIAL SWIRLER

Paul Jourdaine[1,2]*, **Clément Mirat**[1], **Jean Caudal**[2], **Thierry Schuller**[1]
[1] Laboratoire EM2C, CNRS, CentraleSupélec, Université Paris-Saclay,
Grande Voie des Vignes, 92295 Châtenay-Malabry cedex, France
[2] Air Liquide, Centre de recherche Paris Saclay,
Chemin de la Porte des Loges, B.P. 126, 78354 Les Loges en Josas, France
Email: paul.jourdaine@ecp.fr

ABSTRACT

The stabilization of premixed flames within swirling flows produced by an axial-plus-tangential swirler is investigated in an atmospheric test rig. In this system, flames are stabilized aerodynamically away from the solid elements of the combustor without help of any solid anchoring device. Experiments are reported for lean CH4/air mixtures, eventually also diluted with N2, with injection Reynolds numbers varying from 8 500 to 25 000. Changes of the flame shape are examined with OH chemiluminescence and OH laser induced fluorescence measurements as a function of the operating conditions. Particle image velocimetry measurements are used to reveal the structure of the velocity field in non-reacting and reacting conditions. It is shown that the axial-plus-tangential swirler allows controlling the flame shape and the position of the flame leading edge with respect to the injector outlet. The ratio of the bulk injection velocity over the laminar burning velocity U_b/S_L, the adiabatic flame temperature T_{ad} and the swirl number S_0 are shown to control the flame shape and its position. It is then shown that the axial flow field produced by the axial-plus-tangential swirler is different from those produced by axial or radial swirlers. It takes here a W-shape profile with three local maxima and two minima. The mean turbulent flame front also takes this W-shape in an axial plane, with two lower positions located slightly off-axis and corresponding to the positions where the axial flow velocity is minimum. It is finally shown that these positions can be inferred from axial flow velocity profiles under non-reacting conditions.*

INTRODUCTION

Swirling flames are widely used in industrial combustors such as boilers or gas turbines. By imparting a sufficient rotation to the injected flow, a reversal flow often designated as Internal Recirculation Zone (IRZ) develops along the burner axis. Under reactive conditions, hot burnt gases are recirculating inside the IRZ. This recirculation allows sustaining a region filled with hot gases near the burner outlet with low velocities enabling to aerodynamically stabilize the flame away from the solid components of the combustor. Swirling flows expanding at the combustor dump plane also feature outer recirculation zones (ORZ) helping stabilizing the flame. The structure of swirling flows is characterized by highly sheared layers increasing the turbulence level, enhancing mixing and making the flame more compact. Swirling flows allow extending the lean flame blow-off limits [1] and serve to stabilize flames in regions where stretch rates are high [2]. Swirling injectors are widely used technologies to help flame stabilization and increase the volumetric power density of flames [3]. In many labscale experiments, swirling injectors are combined with a central bluff body to help flame stabilization, but in high power applications, the proximity of the flame with this solid component may lead to damages and this additional component is removed ([4, 5, 6]).

Stabilization mechanisms of swirling flames have been the topics of many reviews [7, 8]. It is found that the swirl number, the flow confinement and the diverging cup at the injector outlet are the main geometrical parameters altering the flame topology [9, 10]. Heat losses to the chamber walls are also known to mod-

*Address all correspondence to this author.

ify the flame shape [11, 12].

The swirl number is the most important parameter. It is defined as $S_1 = G_\theta/(RG_z)$, where G_θ is the axial flux of tangential momentum, G_z the axial momentum flux and R is a characteristic radius of the injector. The pressure term in the axial momentum flux G_z is generally neglected and S_1 is given by [13]:

$$S_1 = \frac{\int u_\theta u_z r^2 dr}{r_1 \int u_z^2 r dr} \quad (1)$$

where u_z and u_θ are the axial and azimuthal velocity components and r_1 is the injector outlet radius. The swirl number S_1 remains constant in a tube of constant cross section for an inviscid flow. In practice, it is generally determined at the outlet of the injector. It is known that the swirl number controls the dynamics and topology of swirling flames [7, 13, 14]. To obtain a stable IRZ, the swirl number has to be above a critical threshold value. This value is often found to be around $S_c \sim 0.6$ for radial vanes, but this threshold is not absolute and is sensitive to geometrical details of the injector and of the combustion chamber [15, 16, 17]. It also depends on the structure of the flow field inside the injector and in the injection slits [15, 16]. In many investigations, the swirl number is however not measured but estimated from algebraic expressions in terms of geometrical parameters of the injector.

The flow fields produced by different swirling injectors appear to be qualitatively similar for a given swirl level. Syred *et al.* [18] showed that an IRZ is obtained with a wide set of technologies and that the swirler type makes little difference for the overall recirculating mass flow rate. Gupta [13] however showed that the pressure losses may largely differ and that for swirl numbers $S_1 \leq 0.70$, straight annular vane type swirlers are the more efficient, whereas for higher swirl numbers the use of swirler with curved vanes or swirlers with tangential inlets is more efficient. The choice of the swirler design thus depends on the acceptable pressure drop and on the space available for the swirler. Axial swirlers are more compact than radial or axial-plus-tangential swirlers.

In most practical systems, the swirl number remains fixed [14, 19], but some swirlers have been designed to allow changes of the swirl level [1, 20, 21]. This can be achieved with two different types of technologies. The first types use modifications of the swirler geometry [22]. The second types act on the flow distribution between different injection inlets.

Movable block swirlers belong to the first types. They are used in some labscale burners to change the angle of the flow at the exit of radial or axial swirling vanes [23]. Recent systems were also developed with a step motor control to continuously change the vane angle during operation of the combustor. In other combustors, fluidic systems are preferred. One possibility is the use of axial-plus-tangential swirlers. They allow to continuously change the mass flow rates injected tangentially $\dot{m}_\theta$ and axially $\dot{m}_z$ and thus change the swirl number. Burners like the one used by Claypole *et al.* [21] are based on this principle. The flow-field produced by this type of injector has been investigated for non-premixed flame configurations [24] and in non reacting conditions [15]. The stabilization of fully premixed flames has however not been investigated yet in details with this type of injector.

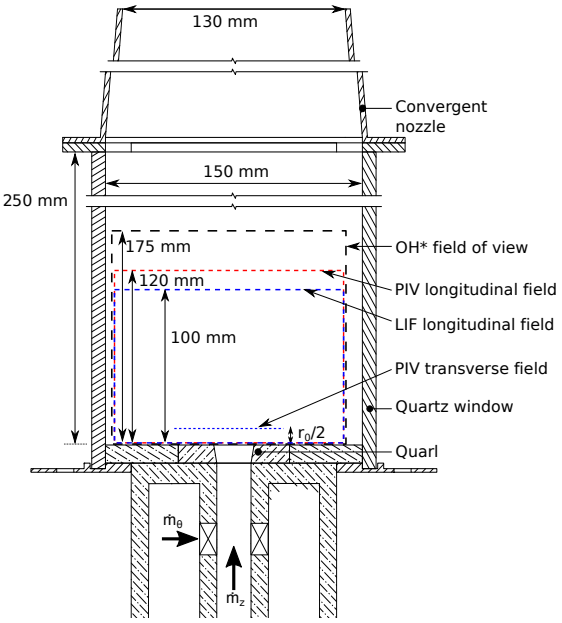

FIGURE 1. OXYTEC atmospheric test-rig.

The purpose of this study is to better understand the stabilization of premixed flames produced by an axial-plus-tangential swirler with a set of optical measurements. The experimental setup and the diagnostics are presented in the next section. Effects of the theoretical swirl number S_0, injection Reynolds number Re and laminar burning velocity S_L on the position of the flame in the chamber are then studied. The structure of the flow field in non-reacting and reacting conditions is finally examined with particle imaging measurements, together with the flame topology deduced from OH laser induced fluorescence measurements.

EXPERIMENTAL SETUP

OXYTEC test-rig

The combustion chamber shown in Fig. 1 is a parallelepiped with a 150 mm square cross section and 250 mm height equipped with four large quartz windows. The system is powered by pure methane and dry air. At the top of the chamber, a converging nozzle with an area contraction ratio of 0.8 is used to fix the recirculation zones of the flow inside the combustion chamber without ambient air entrainment from the surrounding. In the

studied configuration, the nozzle exhausts burnt gases to the atmosphere at ambient pressure.

The injector sketched in Fig. 2 is an axial-plus-tangential entry swirl generator. Assuming an uniform axial flow profile and an azimuthal velocity linearly increasing with the radial distance, the theoretical swirl number S_0 at the injector outlet is ([13], p.168):

$$S_0 = \frac{\pi}{2}\frac{Hr_0}{NlL}\frac{1}{1+\dot{m}_z/\dot{m}_\theta} \quad (2)$$

where $H = 8.9$ mm is the distance separating the tangential injection channels from the burner axis, $r_0 = 10$ mm is the injector radius, $l = 2$ mm and $L = 20$ mm are the width and the height of the N tangential injection channels. By changing the distribution of the mass flow rates injected axially $\dot{m}_z$ and tangentially $\dot{m}_\theta$, the swirl number can be modified during operation without changing the total mass flow rate injected in the combustor. This device was designed to produce theoretical swirl numbers ranging from $S_0 = 0$ to 1.75 with $N = 2$ slits. Experiments were only made for $0.6 < S_0 < 1.2$. Lower or higher values of S_0 did not yield V- or M-shaped flames.

Methane is mixed with the O_2/N_2 or O_2/CO_2 mixture inside the tangential slits of the swirler by a set of three circular holes of 2 mm diameter in each slit. These fuel injection holes are regularly distributed over the height $L = 20$ mm of the slit and are located $d_f = 12$ mm away from the slit outlet. The holes are also inclined with an angle of 30° in the reverse flow direction as shown in Fig. 2(b). This fuel injection system produces a series of highly turbulent jets with a high injection momentum in the main crossflow stream for rapid mixing enhancement. The combustible mixture leaves the swirler through a $r_0 = 10$ mm cylindrical channel and flows into the combustion chamber through an end piece of height $h + e = 33$ mm equipped with a diffuser with a cup angle $\alpha = 10°$. At the outlet of the diffuser cup, the radius is $r_1 = 11.75$ mm.

Mixing of these streams was studied in [25]. Tests were made with small light oil particles (2 micrometers) injected in the different streams and the homogeneity of the flow seeding at the burner outlet was analyzed by laser tomography in axial and transverse planes. It was found that the axial air stream, the tangential air streams and the fuel streams were well mixed at the injector outlet.

Table 1 summarizes the range of operating conditions investigated, where ϕ and P stand for the equivalence ratio and the thermal power. Results presented in this article are restricted to only a selected number of cases. The molar fraction of N_2 in the oxidizer stream is given by $X_{N_2} = n_{N_2}/(n_{N_2} + n_{O_2})$, where n_{N_2} denotes the number of moles of nitrogen and n_{O_2} is the number of moles of oxygen ($X_{N_2} = 0.79$ when air is used as oxidant). The Reynolds number $Re = 2U_b r_0/\nu$ is calculated with the bulk

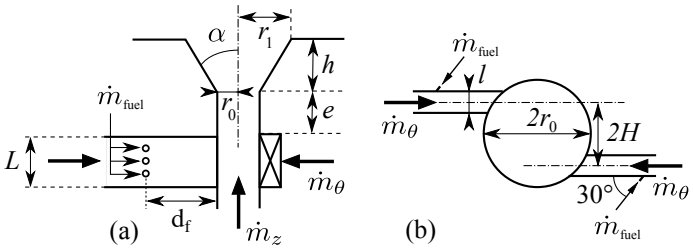

FIGURE 2. Sketch of the injector with the main dimensions. (a) Axial cut. (b) Transverse cut through the swirler.

velocity U_b of the combustible mixture through the injection tube of radius $r_0 = 10$ mm and the kinematic viscosity ν of this mixture. The velocity U_b is given for injection at $p = 1$ atm and $T_u = 300$ K.

Bronkhorst mass flow controllers are used to adjust the axial $\dot{m}_z$ and tangential $\dot{m}_\theta$ mass flow rates injected. The adiabatic flame temperature T_{ad} and laminar burning velocity S_L are calculated with an homemade solver REGATH [26] with the GRI 3.0 mechanism. In all experiments, the combustible mixture leaves the injector at ambient temperature $T_u = 300$ K. Care was taken to thermalize the injection lines of the different gases and measurements were all carried out twenty minutes after ignition of the combustion chamber.

Diagnostics

Optical diagnostics are used to characterize the flow and flame patterns. The shape taken by the flames is investigated with OH* chemiluminescence images. The OH* signal is a good tracer of the reaction zone for lean stoichiometric premixed flames [27]. These images are recorded with a 16 bit intensified CCD camera (ICCD, Princeton, PI-MAX4, 1024 × 1024 pixels) equipped with an UV objective lens (Nikkor 105 mm) and a 10 nm bandpass filter centered at 310 nm (Asahi XBPA310-Bandpass) to collect the OH* signal. The OH* field of view of the ICCD camera is shown in Fig. 1. The mean turbulent flame topology is deduced from averages of 100 snapshots with a camera gate width of 20 ms for each image.

Planar Laser Induced Fluorescence measurements of the hydroxyl radical (OH-PLIF) in an axial plane are also used to infer the location of the burnt gases. The hydroxyl radical is formed in the reaction zone and persists in the hot burnt gases by dissociation of water at high temperature [28]. In premixed flames, the OH gradient is a good tracer of fresh/burnt gases interface [29, 30, 31]. A dye laser (Continuum, ND6000) delivering 10 mJ per pulse is used with Rhodamine 590 diluted in a methanol solvent and pumped by a Nd:YAG laser (Continuum, Precision) operated at a 10 Hz repetition rate. The laser is tuned to the Q1(6) transition of the (1,0) band of the A2-X2 system of OH at 282.935 nm. The fluorescence signal is collected with the same camera used for the OH* images but with a smaller field of view

TABLE 1. Range of operating conditions explored.

ϕ	P [kW]	S_L [cm.s^{-1}]	U_b [m.s^{-1}]	Re	X_{N_2}	T_{ad} [K]	S_0
0.7-1.0	5-20	16.5-57	6.5-22	6500-28000	0.75-0.85	1870-2360	0.6-1.2

indicated in Fig. 1. The axial laser sheet has a 10 cm height and a 0.5 mm thickness.

A set of 1500 images were taken at a 5 Hz repetition rate to deduce the probability of presence of the burnt gases from the OH-PLIF measurements. It was verified that statistical convergence of the mean and root-mean-square (rms) components of the signal was achieved. Then, the instantaneous images were binarized above a threshold value corresponding to 15% of the maximum pixel intensity. Averages of the binarized images yield the probability of presence of hot burnt gases. This method is used to separate the hot burnt gases from the fresh ones. The burnt gases that are cooled by heat losses are not accounted for with this technique. In the regions filled with burnt gases at low temperature, the chemical equilibrium of burnt gases is shifted towards H_2O at the expense of the OH radical due to the drop of enthalpy [32]. The burnt gases probability deduced from OH-PLIF images in these zones is falsely attributed to a zero value. Therefore, these OH-PLIF experiments yield the probability of presence of burnt gases only when they are sufficiently hot.

The flow field inside the combustor was studied with Particle Image Velocimetry (PIV) measurements. The flow is in this case seeded with micro-metric oil particles for the non-reacting cases [33] and with micro-metric ZrO_2 particles (Fisher Scientific Zirconium (IV) oxyde, Z/1850/50) for the reacting cases. Particles are injected in the axial stream (Fig. 2). The PIV system features a 2 x 400 mJ Nd:YAG laser doubled at 532 nm operated at 10 Hz (Continuum, Powerlite SL3-PIV) and a 1600 $\times$ 1200 pixels CCD camera (Dantec Dynamics, Flow Sense). Measurements are done in an axial light sheet crossing the burner axis and in transverse planes as indicated in Fig. 1. The laser sheet has a 130 mm width and a relatively wide thickness of 1 mm to minimize out of sheet particle displacements of the swirling flow between the two laser pulses. A thousand of image pairs are recorded at 10 Hz for each operating conditions to allow statistical convergence of the mean and root-mean-square (rms) components of the velocity field. Pairs of images are separated by 15 μs. This duration corresponds to a maximum particle displacement of 4 pixels between the image pairs taken by the CCD camera. A two passes window deformation technique is applied to deduce the velocity field from the cross-correlation of two tomographic snapshots.

FLAME STABILIZATION

Effects of the injection conditions on the shape and position taken by the flame produced by the axial-plus-tangential swirler are now analyzed. Effects of the swirl number S_0 are investigated first.

Figure 3 shows the OH* signal recorded for five CH_4/air flames featuring the same equivalence ratio $\phi = 0.95$ and thermal power $P = 13$ kW, but different swirl levels varying from $S_0 = 0.70$ to $S_0 = 1.0$. It is known that the flame shape is greatly altered when the swirl number changes (see for example [20] for a radial swirler). For a swirl number lower than $S_0 = 0.70$, the flame is highly turbulent with a lifted pattern far above the burner and occupies a large volume. For $S_0 = 0.70$, combustion is more compact and takes place closer to the injector rim, but the flame switches intermittently between a V-shape stabilized at the burner outlet and a lifted pattern far away from the burner. Between $0.75 \leq S_0 < 0.95$, the flame takes a well defined V-shape [11, 34] with a flame leading edge lying above the burner outlet $z_f > 0$. Figure 3(c) shows the reference flame obtained for $S_0 = 0.85$ that will be further examined with PIV and OH-PLIF diagnostics. The flame leading edge position lies in this case at $z_f/r_0 = 1$. For $S_0 = 1.0$, the flame takes a tulip-shape in Fig. 3(e) as designated in [35] with a leading edge protruding inside the injector ($z_f/r_0 < 0$). For higher swirl numbers $S_0 > 1.0$, the flame keeps a tulip-shape but becomes more elongated for increasing values of S_0, until the flame is again lifted far away above the injector as in Fig. 3(a). In this case, a highly turbulent flame again occupies a large volume with a lifted pattern.

Flames observed for $S_0 \leq 0.7$ and $S_0 \geq 1.0$ at $P = 13$ kW are not interesting from a practical point of view because they strongly interact with the combustion chamber sidewalls or the injector solid pieces. They are highly unsteady and thus may damage the combustor.

Experiments are repeated for different thermal powers P by increasing the bulk flow velocity U_b at a fixed equivalence ratio $\phi = 0.95$. Figure 4 shows results for CH_4/air flames at a thermal power $P = 20$ kW when the swirl number is varied. Once again a small change of the swirl number alters the flame shape. V-shaped flames are obtained for $0.7 \leq S_0 \leq 0.9$. For $S_0 \geq 0.95$, tulip-shaped flames are observed. When the swirl number increases, the flame leading edge position z_f moves upstream towards the injector outlet: $z_f/r_0 = 3.9$ for $S_0 = 0.70$, $z_f/r_0 = 2.3$ for $S_0 = 0.75$ and $z_f/r_0 = 1.3$ for $S_0 = 0.85$. At higher swirl numbers, the flame root protrudes inside the injector.

The axial-plus-tangential swirler allows continuously changing the swirl number and eases controlling the shape and position of the flame inside the combustor for the different levels of power tested. Increasing the swirl number moves the flame upstream. Flame stabilization is also found to be slightly

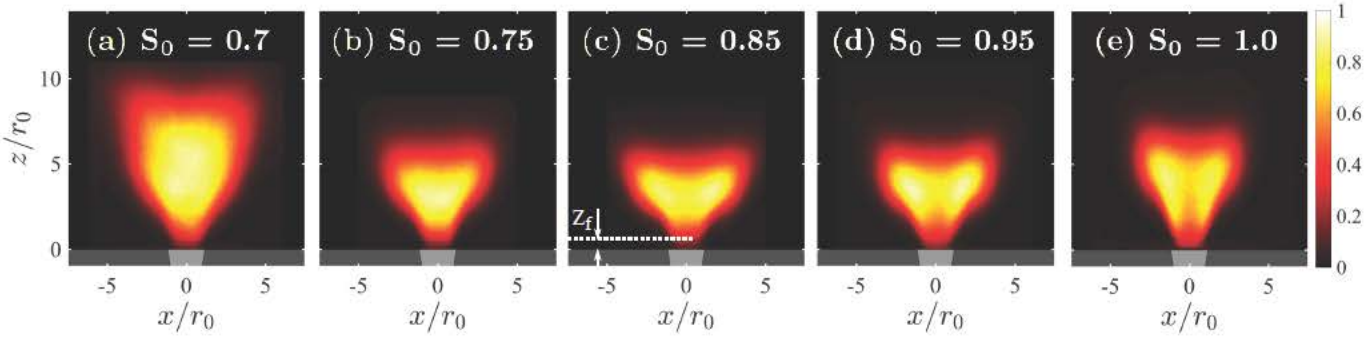

FIGURE 3. OH* images of CH_4/air flames, $\phi = 0.95$, $P = 13$ kW, $Re = 18000$, $U_b = 14.3$ m/s, $U_b/S_L = 39$ and varying swirl numbers S_0.

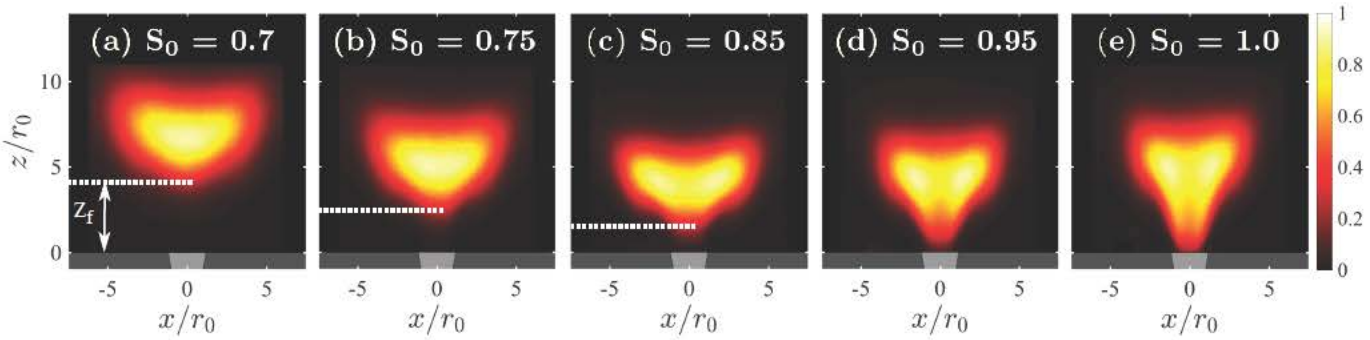

FIGURE 4. OH* images of CH_4/air flames, $\phi = 0.95$, $P = 20$ kW, $Re = 27800$, $U_b = 21.9$ m/s, $U_b/S_L = 59$ and varying swirl numbers S_0.

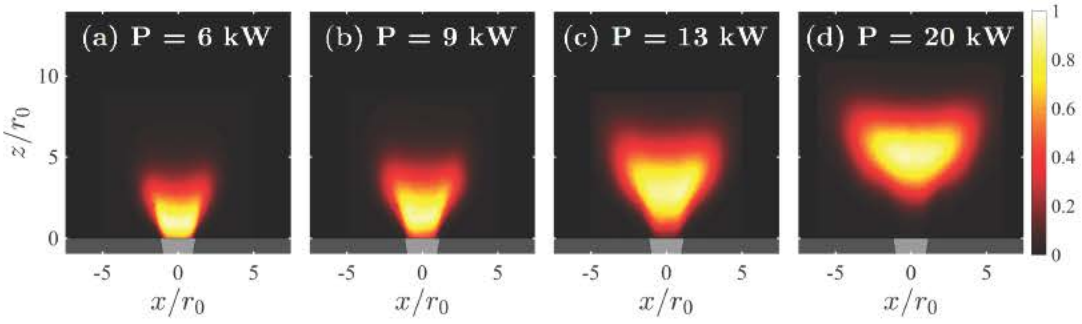

FIGURE 5. OH* images of CH_4/air flames, $\phi = 0.95$, $S_0 = 0.75$ and varying thermal power P.

sensitive to the injection Reynolds number.

Figure 5 shows the OH* light distribution for flames featuring a fixed swirl number $S_0 = 0.75$ with injection Reynolds numbers varying from $Re = 8350$ ($P = 6$ kW) to $Re = 27800$ ($P = 20$ kW). Increasing the injection Reynolds number yields larger flames and also alters the flame position inside the chamber. The lift-off height of the flame leading edge z_f increases with the injection Reynolds number. The flame keeps a V-shape in all images in Fig. 5, but the flame leading edge protrudes inside the injector $z_f < 0$ in Figs. 5(a) and (b) at low Reynolds numbers $Re < 15000$. For higher Reynolds numbers, the flame leading edge is stabilized above the injector $z_f > 0$ close to the outlet at $P = 13$ kW and a bit further downstream at $P = 20$ kW.

The same experiments were repeated for swirl numbers $0.6 < S_0 < 1.0$. It was found that at high Reynolds numbers, the range of swirl numbers where the flame is well stabilized above the burner outlet widens. For example at $P = 20$ kW, V-shaped flames are well stabilized above the burner for $0.70 \leq S_0 \leq 0.95$. At $P = 13$ kW, well stabilized V-shaped flames could only be obtained for $0.75 \leq S_0 \leq 0.90$. At low injection Reynolds numbers $Re < 13000$, it was not possible to stabilize CH_4/air flames at this equivalence ratio $\phi = 0.95$ with a leading edge outside the injector over the range of swirl levels that can be reached with this axial-plus-tangential swirler. Above the threshold level $Re > 13000$, varying the swirl number S_0 allowed controlling the position of the flame leading edge with respect to the injec-

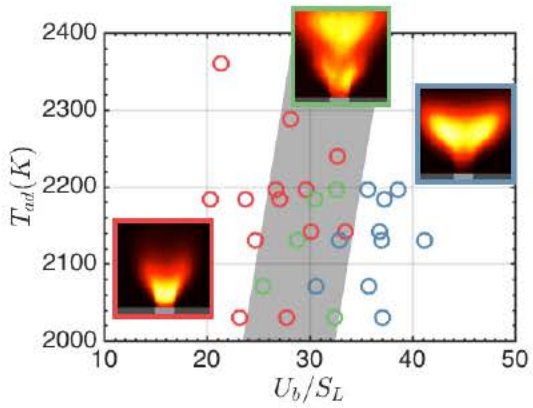

FIGURE 6. Position of the leading reaction edge of N_2-diluted CH_4/air lean flames at $S_0 = 0.75$ as a function of T_{ad} and U_b/S_L. The flame leading edge is located inside $z_f/r_0 < 0$ (red) or outside $z_f/r_0 > 0$ (blue) the injector. Green symbols indicate undetermined states with oscillations between these two states. The grey zone roughly delineates the transition region where it is difficult to safely determine the leading edge flame position.

tor outlet. Increasing the swirl number brings the flame closer to the burner outlet. Increasing the Reynolds number broadens the range of swirl numbers where the flame is well stabilized.

At this stage, one may already conclude that the position and the shape of CH_4/air flames at $\phi = 0.95$ stabilized by this axial-plus-tangential device can easily be controlled by adjusting the swirl number S_0 and the bulk injection velocity U_b. Increasing the bulk velocity increases the lift-off height z_f of the flame leading edge above the injector whereas increasing the swirl number decreases this height.

Experiments are now conducted with $CH_4/O_2/N_2$ flames at different equivalence ratios ϕ and dilution rates X_{N_2} to obtain mixtures featuring different adiabatic flame temperatures T_{ad} and laminar burning velocities S_L. Figure 6 maps the position of the flame leading edge as a function of the adiabatic flame temperature T_{ad} and the ratio of the bulk velocity U_b to the laminar burning velocity S_L.

Figure 6 indicates that swirling flames at $S_0 = 0.75$ featuring a leading edge above the injector outlet are observed when the ratio U_b/S_L is high enough (blue symbols). If this ratio is too low, the flame leading edge protrudes inside the injector (red symbols). Conditions corresponding to a flame intermittently inside or outside the injector are designated by the green symbols. The intermediate zone colored in grey in Fig. 6 roughly delineates the boundaries of these different zones. The critical values U_b/S_L of the boundaries of the transition zone increase with the adiabatic flame temperature. Increasing T_{ad} brings the flame closer to the injector. For $T_{ad} = 2150$ K, flames with a leading edge front well stabilized above the injector are found for $U_b/S_L > 34$. This critical value increases to $U_b/S_L > 36$ for $T_{ad} = 2250$ K. These data are obtained for $S_0 = 0.75$. A shift of the critical boundaries for U_b/S_L to higher values is found when the swirl number S_0 is increased and conversely (not shown here).

This set of experiments reveals that the flame shape and the location of the leading edge front with respect to the burner outlet can easily be controlled with the axial-plus-tangential swirler for a large range of injection conditions by fixing the ratio of the bulk velocity to the laminar burning velocity U_b/S_L, the adiabatic flame temperature T_{ad} and the swirl number S_0. Increasing S_0 or T_{ad} moves the flame upstream. Increasing the ratio U_b/S_L increases the flame lift-off height.

FLOW AND FLAME TOPOLOGY

The flow field above the injector is now investigated under non-reacting conditions in axial and transverse planes. The swirl number S_1 is deduced and compared to theoretical estimates S_0. PIV and OH-PLIF measurements are then carried out in the axial plane under reacting conditions. The two diagnostics are combined to reveal the position of the flame within the aerodynamic field. A comparison between the velocity fields under reactive and non-reactive conditions is finally made. For the remaining part of the study, CH_4/air flames with an equivalence ratio $\phi = 0.95$ and an injection Reynolds number $Re = 18000$ ($P = 13$ kW) are considered. Only the swirl number S_0 is varied.

Non-reacting conditions

Figure 7 shows the velocity fields in the axial plane passing through the center of the burner when the injector is operated at swirl numbers $S_0 = 0.70$, 0.85 and 1.0 calculated with Eq. (2). The black line in Fig. 7 delineates the position of the lower boundary of the IRZ where $u_z = 0$. In these experiments, the injected air volumetric flow rates are compensated for the absence of fuel injection to match the same bulk velocity U_b of the reacting operating conditions at $\phi = 0.95$ and $P = 13$ kW ($Re = 18000$).

The topology of the flow field near the burner outlet is greatly altered when the swirl number S_0 changes in Fig. 7. When $S_0 = 0.70$, there is no IRZ in the PIV view field (Fig. 7, top image). Only one jet is present at the outlet of the burner with the highest velocity along the burner axis. A small asymmetry can also be distinguished in the velocity field near the combustor flange for this swirl number. This is due to an imperfect machining of the swirler tangential slits. As the swirl number increases, the velocity field becomes more symmetric and the asymmetry disappears. For a higher value corresponding $S_0 = 0.75$, an IRZ appears around the burner axis (not shown here). When the swirl number is further increased to $S_0 = 0.85$, the swirling flow now exhibits three regions with high velocities at the burner outlet (Fig. 7, middle image). The first lies again along the center axis

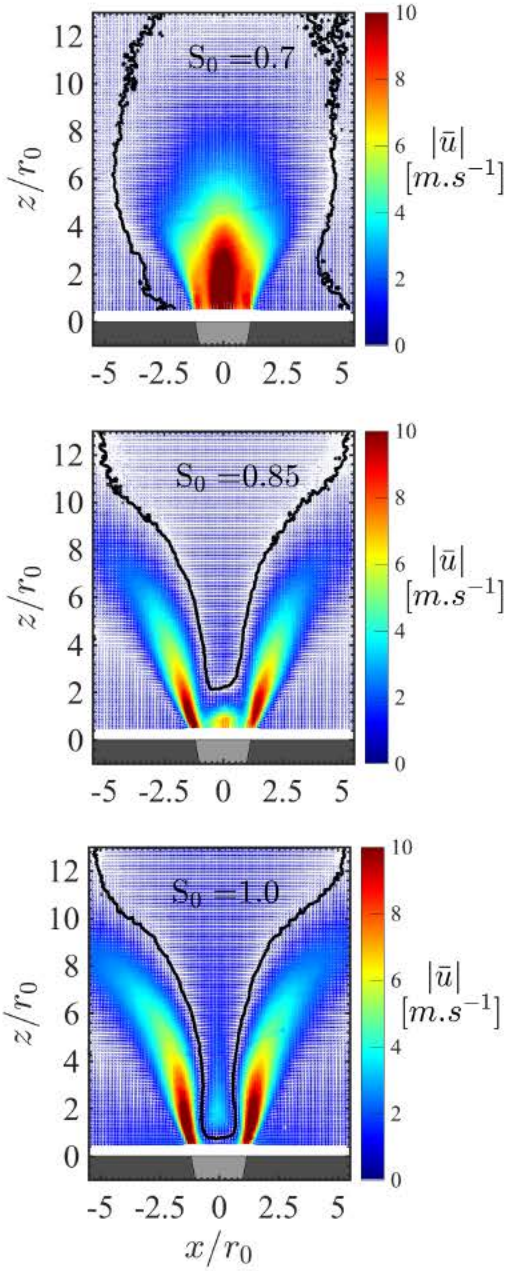

FIGURE 7. 2D velocity fields in non-reacting conditions measured in the axial plane passing through the center of the injector. The black line delineates the position where the axial velocity is zero, $u_z = 0$ m.s^{-1}. $U_b = 14.3$ m.s^{-1}, $Re = 18000$, $S_0 = 0.70$ (top), 0.85 (middle) and 1.0 (bottom).

of the injector, but the highest velocities are reached along two side branches featuring an angle close to that of the injector cup outlet. When S_0 is further increased to 1.0, the IRZ lowers and gets closer to the burner outlet, while the central jet along the axis weakens (Fig. 7, bottom image). The stagnation point of the flow along the burner axis lowers from $z_{st}/r_0 = 2$ for $S_0 = 0.85$

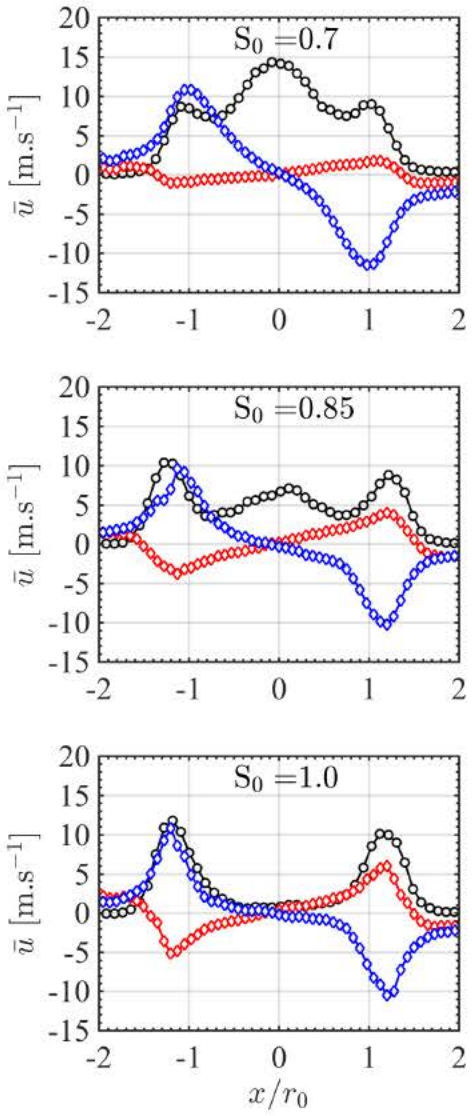

FIGURE 8. Axial (black), radial (red) and tangential (blue) velocity profiles at $z/r_0 = 0.5$ extracted from the PIV fields presented in Fig. 7.

to $z_{st}/r_0 = 0.8$ for $S_0 = 1.0$. These measurements confirm that the position of the IRZ is controlled by the swirl number S_0.

Assuming a mean axisymmetric flow field structure (see Figs. 3 to 5), PIV measurements in transverse planes are used to get the azimuthal velocity component of the flow. Figure 8 plots the axial (black), radial (red) and azimuthal (blue) velocity profiles extracted at $z/r_0 = 0.5$ for the flow conditions studied in Fig. 7. One now clearly identifies three local maxima in the axial velocity profiles for $S_0 = 0.70$ and 0.85. These profiles reveal three jets with high axial velocities at the burner outlet and take the shape of a W for $z/r_0 = 0.5$. For $S_0 = 0.70$, they however quickly merge downstream and form only one jet as shown

TABLE 2. Swirl numbers: S_1 determined with Eq. (1) and the velocity components measured at $z/r_0 = 0.5$ and $z/r_0 = 2.0$. S_0: theoretical estimates with Eq. (2). $Re = 18\,000$.

S_0	0.70	0.85	1.00
S_1 at $z/r_0 = 0.5$	0.76	0.92	0.94
S_1 at $z/r_0 = 2.0$	0.80	0.89	0.91

in the top image in Fig. 7 for $z/r_0 > 2$. When S_0 increases the peak axial velocity along the burner axis progressively drops and vanishes for $S_0 = 1.0$ in Fig. 8. This drop is accompanied by a progressive increase of the peak radial velocity, while the maximum azimuthal velocity remains roughly constant and equal to $u_\theta = 10$ m.s^{-1} when S_0 changes from 0.70 to 1.0. Only the radial position where this maximum is reached and the shape of the azimuthal velocity profile change. When $S_0 = 0.70$, the azimuthal component has a Rankine like profile with a maximum located at $|x|/r_0 = 1.0$. At higher swirl numbers $S_0 = 0.85$ and 1.0, the azimuthal velocity profile cannot fully develop and a large dead zone with low velocities is present at the center of the injector. The highest azimuthal velocities are found in these cases at $|x|/r_0 \simeq 1.2$ indicating that the swirling jet spreading angle increases when the swirl number increases.

The velocity profiles in Fig. 8 are now used to determine the swirl number S_1 with Eq. (1). Values of the swirl number measured at $z/r_0 = 0.5$ and $z/r_0 = 2.0$ are presented in Table 2. The measured values S_1 are close to the theoretical estimates S_0. Relative differences are lower than 10%. However, the measured values for S_1 are higher than the theoretical estimates for $S_0 = 0.70$ and 0.85, whereas for $S_0 = 1.0$, the value found for S_1 is lower. For $S_0 = 0.85$ and 1.0, one may note that the measured values S_1 are close even though the injection conditions have changed and the flow structure is quite different in Fig. 7 between these two cases.

When injection is made at $S_0 = 0.85$, the axial velocity $u_z = 7$ m.s^{-1} along the burner axis corresponds to a local maximum in Fig. 8. When injection is made at $S_0 = 1.0$, the axial velocity now features a minimum $u_z = 0.7$ m.s^{-1} along the burner axis. The flame shapes also clearly differs in Fig. 3. The flame has a V-shape at $S_0 = 0.85$ and tulip-shape at $S_0 = 1.0$. One may conclude that the measured value S_1 of the swirl number at the burner outlet is not the best indicator of the topology of the flow field for this type of injector. The theoretical swirl number calculated here with Eq. (2) yields a better indication of the flame shape than the measured value given by Eq. (1).

It is also worth noticing that a much higher swirl number S_1 is needed to trigger vortex breakdown than for a burner equipped with an axial or radial swirler. In many radial or axial swirlers, a critical threshold value of $S_1 \simeq 0.6$ is generally enough to trigger vortex breakdown and get a stable IRZ [7, 13, 20]. With the axial-plus-tangential swirler used in this study, the IRZ only appears at higher values when $S_1 \geq 0.75$ (Fig. 7). This is probably due to the presence of the axial central jet with high velocities produced by this axial-plus-tangential injection device for swirl numbers $S_1 < 1.0$. This central jet delays the birth of the IRZ.

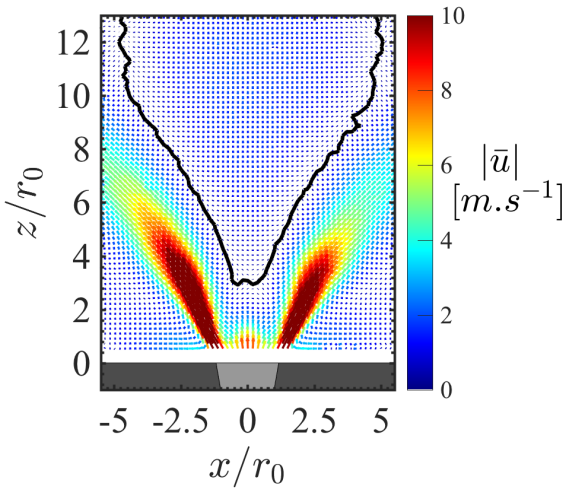

FIGURE 9. Velocity field in reacting conditions measured in the axial plane crossing through the center of the injector. The black line delineates the position where the axial velocity is zero, $u_z = 0$. $U_b = 14.3$ m.s^{-1}, $S_0 = 0.85$, $Re = 18\,000$, $\phi = 0.95$.

Reacting conditions

The structure of the velocity field is now investigated with combustion. Figure 9 show the trace of the velocity field in the axial plane under reacting conditions for the same injection conditions as those presented in Fig. 7 for non-reacting conditions at $S_0 = 0.85$. Qualitatively, the two figures are similar. These figures highlight the same flow topology and velocity levels.

Figure 10 compares the axial and radial velocity components in non-reacting (blue circles) and reacting conditions (red diamonds). These profiles are extracted from Fig. 7 and 9 at different heights $z/r_0 = 0.5$, 1.5 and 3.0 above the injector. The radial u_r and axial u_z velocity components with and without combustion are close near the burner outlet at $z/r_0 = 0.5$. The only differences are the slightly higher values of the maxima reached by the axial and radial velocities in the reacting case. Differences increase also for $x/r_0 > 1.5$ due to thermal expansion of the flow in the reacting case. The two non-reacting velocity components u_r and u_z decrease faster with the distance to the injector than for the reacting case. At $z/r_0 = 3.0$, differences between reacting and non-reacting velocity profiles increase. This is again due to the thermal expansion of the gases. Flow velocities downstream the flame front take higher values in the reacting case. The opening angle of the external jet of high velocity is also higher in the reacting case. The radial position where the maximum veloc-

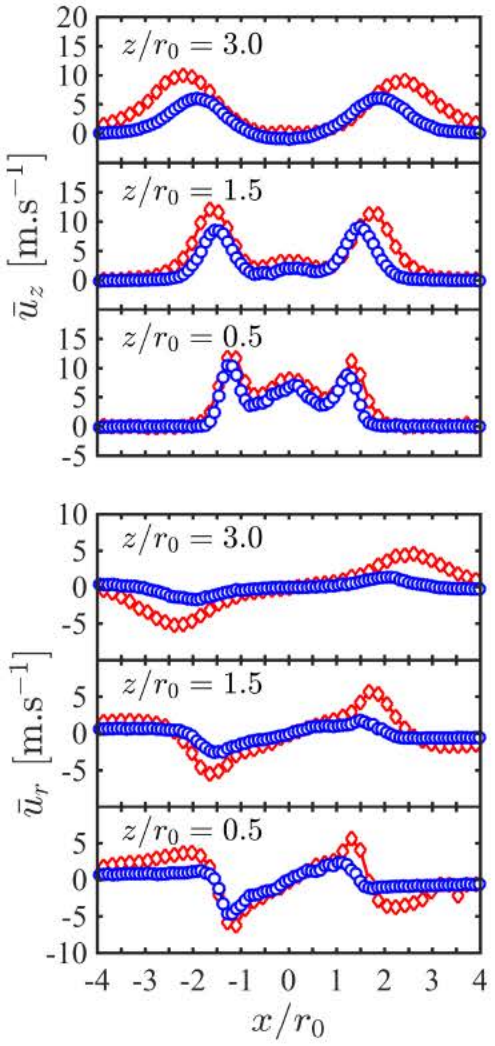

FIGURE 10. Axial u_z (top) and radial u_r (bottom) velocity profiles in reacting (red diamonds) and non-reacting (blue circles) conditions with $S_0 = 0.85$ at $z/r_0 = 0.5$, 1.5 and 3.0.

ity is reached is in both cases located between the inner shear layer (ISL) and the outer shear layer (OSL). For $z/r_0 = 3.0$, this maximum is reached at $|x|/r_0 = 2.3$ in the reacting case and at $|x|/r_0 = 1.9$ in the non-reacting case.

A close examination between Figs. 7 and 9 also reveals that the IRZ moves upstream when the flame is present. The stagnation point of the IRZ is found along the burner axis at $z_{st}/r_0 = 2.5$ in reacting conditions and at $z_{st}/r_0 = 2.1$ in non-reacting conditions. The main conclusion is that flows with and without combustion are very similar at the injector outlet. The W shape of the axial velocity profiles for $S_0 < 1.0$ is confirmed. One may then infer the flow topology in reacting conditions by conducting easier experiments in non-reacting conditions. This feature has been verified for swirl numbers between $0.70 \leq S_0 \leq 1.0$ and is

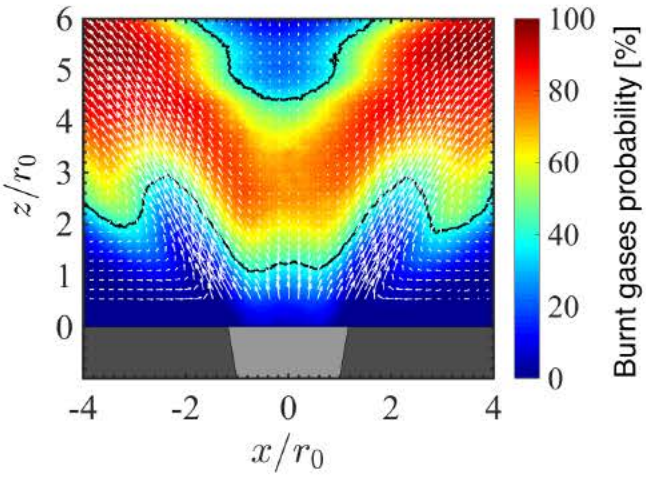

FIGURE 11. Probability of presence of hot burnt gases in the axial plane overlaid with the corresponding velocity field. The black line delineates the positions where the hot burnt gases are present 40% of the time. $\phi = 0.95$, $Re = 18000$, $S_0 = 0.85$. Spacial resolution: 8.55 pixels/mm.

reminiscent to that known for radial or axial swirlers [36].

OH-PLIF measurements are now used to investigate the structure of the flame in the axial plane crossing the injector axis. The probability of presence of hot burnt gases combined with the previous velocity measurements are plotted in Fig. 11. The hot burnt gases are indicated in red in this figure. The outer recirculation zone (ORZ) filled with cooled burnt gases appear in blue as the fresh gases. For $S_0 = 0.85$, the flame takes a V-shape like structure with also a reaction layer that is slightly protruding in the OSL of the flow as described in [37]. The combustion takes mainly place in the ISL formed by the jet flow exhausting the injector and the IRZ. Reaction also takes also place intermittently in the OSL of the jet flow and the ORZ. An M-shape like structure with two well stabilized reaction layers in the ISL and OSL is found for $0.75 \leq S_0 \leq 0.90$.

Figure 11 also reveals that the highest probability to find the flame leading edge position does not lie on average along the burner axis, but this position is slightly off-set in the radial direction. This information could not be detected with the OH* chemiluminescence images shown in Figs. 3 and 4 due to the line of sight integration of the light originating from the flame. Attempts were made to retrieve this feature with an Abel inversion of the chemiluminescence data, but the singularity of this transformation close to the burner axis resulted in a too weak SNR to detect anything in the region close to the burner axis.

Figure 12 plots the mean axial velocity profile (black solid line) extracted from Fig. 9 together with the corresponding root-mean-square values (red solid line) and the burnt gases probability of presence (black dotted line) obtained for the same condi-

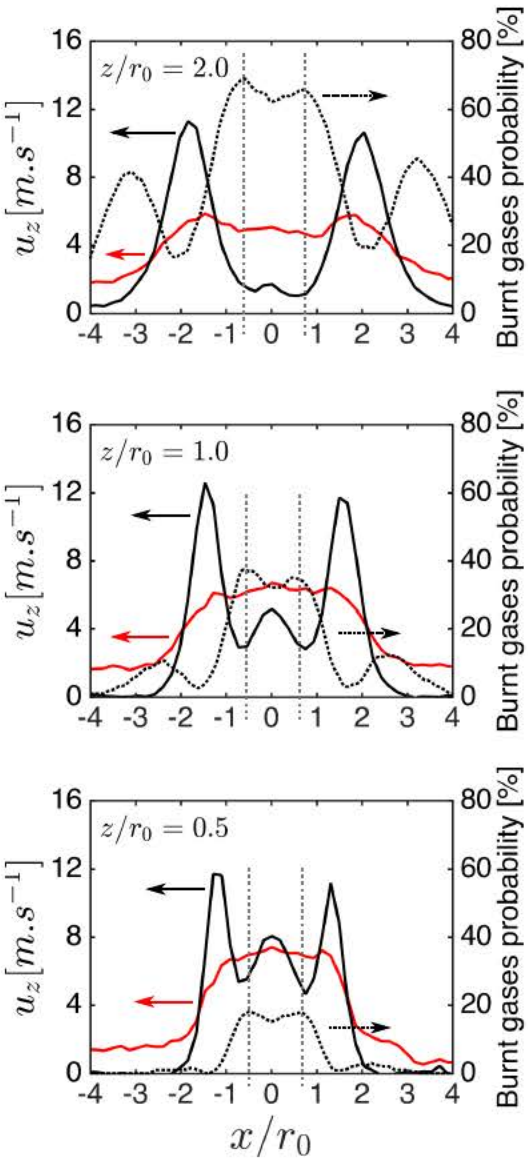

FIGURE 12. Axial velocity (-), axial rms velocity (-) and burnt gases probability of presence (---) extracted from the Fig. 9 and 11 respectively at $z/r_0 = 2.0$ (top), $z/r_0 = 1.0$ (middle) and $z/r_0 = 0.5$ (bottom).

tions and extracted from the Fig. 11 at $z/r_0 = 0.5$, 1.0 and 2.0. Figure 12 makes a clear link between the lowest values of the mean axial velocity and the highest values of probability of presence of burnt gases as indicated by the dashed vertical lines. It confirms that the flame leading edge statistically preferentially lies in the zones of low velocity comprised between the central axis where the axial velocity reaches a local maximum and the local high values of the axial velocity reached by the swirling jet in the ISL. As a conclusion, the transverse profiles for the probability of presence of burnt gases follow the W shape axial velocity profiles and the flame also takes a W-shape around the burner axis. Experiments conducted at swirl numbers $0.75 \leq S_0 \leq 0.95$ where the flame is stabilized above the injector outlet section also yielded the same results with a W flame shape profile around the burner axis.

The root-mean-square values (rms) of the axial velocity component provide valuable information on the turbulence level reached by the flow above the injector. The flow produced by the axial-plus-tangential swirler is found to be highly turbulent. The mean ($\bar{u}_z$) and rms (u'_z) axial velocity levels averaged over the burner section reach $\bar{u}_z = 7.0$ m.s^{-1} and $u'_z = 6.0$ m.s^{-1} at $z/r_0 = 0.5$ and $\bar{u}_z = 5.9$ m.s^{-1} and $u'_z = 4.5$ m.s^{-1} at $z/r_0 = 2.0$ in Fig. 12. The rms values take about the same values as the mean components. The same features were observed for the cold flow conditions and for all velocity components and all injection conditions explored in this work.

Attempts were made to elucidate the mechanisms controlling flame stabilization in this highly turbulent flow above the injector outlet. It has already been indicated that the highest probability of presence of the flame leading edge systematically lies slightly off-set in the radial direction with respect to the burner axis and this position always corresponds to the lowest local mean axial velocity. Attempts were made to deduce the turbulent burning velocity from the data plotted in Fig. 11, but the probability of presence of burnt gases remains relatively weak at $z/r_0 = 1.0$ which corresponds to the height above the burner where the flame leading edge position has been deduced from the chemiluminesence data plotted in Fig. 3(c). This probability never exceeds 40% in Fig. 12 at $z/r_0 = 1.0$. This denotes again a highly intermittent flame and this was confirmed by examining individual OH-PLIF snapshots. A spectral analysis of the data gathered also revealed a coherent structure at 820 Hz for the injector used without diverging cup at the same flow operating conditions. In this case, the flame was not well stabilized close to the injector nozzle outlet as in this study conducted with a cup angle of 10°. This coherent signal however disappeared in the data gathered with injector with the cup angle of 10°. There is yet no satisfactory explanation for the flame leading edge stabilization. Further studies of the instantaneous velocity fields will be conducted to try to understand the mechanisms controlling the stabilization of the flame.

CONCLUSION

The stabilization of swirling premixed CH_4/air flames produced by an axial-plus-tangential swirler has been studied experimentally. Chemiluminescence images have first been used to characterize effects of the swirl number S_0, the injection Reynolds number Re, the laminar burning velocity S_L and the adiabatic flame temperature T_{ad} on the flame shape and its position with respect to the injector outlet. It was first found that operating the system with swirl numbers ranging between

$0.70 < S_0 < 0.90$, an injection Reynolds number $Re = 18\,000$ and an equivalence ratio $\phi = 0.95$ allowed to aerodynamically stabilize CH_4/air flames in a V-shape close to the burner outlet with a flame leading edge located outside the injector. It was then found that the position and the shape of the flame produced with this axial-plus-tangential swirler are controlled by the ratio of the bulk velocity to the laminar burning velocity U_b/S_L, the adiabatic flame temperature T_{ad} and the swirl number S_0 for a range of injection Reynolds numbers covering $Re = 8\,500$ to $28\,000$. Selecting the right values for these parameters allows to stabilize the flame close to the burner without interacting with the combustor or injector walls. Increasing the swirl number S_0 or the adiabatic flame temperature T_{ad} decreases the lift-off distance of the flame. Increasing the ratio U_b/S_L increases this distance.

The structure of the non-reacting flow revealed by PIV measurements indicate that the axial velocity profile takes a W-shape at the injector outlet for swirl numbers $S_0 < 1.0$. This particular structure of the flow field allows to control the position of the IRZ by varying the swirl number S_0. The swirl number S_0 calculated with Eq. (2) was also shown to take about the same values as those deduced from the measurements made at the injector outlet. The parameter S_0 was however found to yield a better indication of the shape taken by the flame than the measured values of the swirl number. It was also found that the axial-plus-tangential injector needs to be operated at higher swirl number values than radial or axial swirling vanes to produce a stable IRZ. Stable IRZ were found here for $S_1 > 0.8$. It was found that the high axial velocity along the burner axis delays the formation of a stable IRZ.

The flame structure and the corresponding velocity field under reacting conditions produced by the axial-plus-tangential swirler have finally been investigated with OH-PLIF and PIV measurements. These diagnostics revealed an axial velocity distribution with a W-shape profile and an off-axis statistical average position of the flame leading edge located between the burner axis and the ISL of the swirling jet. The position of the flame leading edge corresponds to the position where the W-shape axial velocity profile features a local velocity minimum at about the mid-width of the injector. This study shows that an axial-plus-tangential swirler allows to easily control the leading edge position and the shape of premixed swirling flames. This type of device yields flames aerodynamically stabilized above the injector for a relatively large range of injection Reynolds numbers.

ACKNOWLEDGMENT

This work is supported by the Air Liquide, CentraleSupélec and CNRS Chair on oxy-combustion and heat transfer for energy and environment and by the OXYTEC project (ANR-12-CHIN-0001) from l'Agence Nationale de la Recherche. We also would like to thank the technical staff of EM2C for their assistance during the design and construction of the experimental setup.

References

[1] Feikema, D., Chen, R.-H., and Driscoll, J. F., 1990. "Enhancement of flame blowout limits by the use of swirl". *Combustion and Flame,* ***80***(2), pp. 183 – 195.

[2] Stöhr, M., Boxx, I., Carter, C., and Meier, W., 2011. "Dynamics of lean blowout of a swirl-stabilized flame in a gas turbine model combustor". *Proceedings of the Combustion Institute,* ***33***(2), pp. 2953 – 2960.

[3] Döbbeling, K., Knöpfel, H. P., Polifke, W., Winkler, D., Steinbach, C., and Sattelmayer, T., 1996. "Low-NOx premixed combustion of MBtu fuels using the ABB double cone burner (EV burner)". *Journal of Engineering for Gas Turbines and Power,* ***118***(1), pp. 46–53.

[4] Biagioli, F., 2006. "Stabilization mechanism of turbulent premixed flames in strongly swirled flows". *Combustion Theory and Modelling,* ***10***(3), pp. 389–412.

[5] Biagioli, F., Güthe, F., and Schuermans, B., 2008. "Combustion dynamics linked to flame behaviour in a partially premixed swirled industrial burner". *Experimental Thermal and Fluid Science,* ***32***(7), pp. 1344 – 1353. Fifth mediterranean combustion symposium.

[6] Paschereit, C. O., Flohr, P., Knöpfel, H., Geng, W., Steinbach, C., Stuber, P., Bengtsson, K., and Gutmark, E., 2002. "Combustion control by extended EV burner fuel lance". In ASME Paper GT2002-30462.

[7] Syred, N., 2006. "A review of oscillation mechanisms and the role of the precessing vortex core (PVC) in swirl combustion systems". *Progress in Energy and Combustion Science,* ***32***, pp. 93 – 161.

[8] Rawe, R., and Kremer, H., 1981. "Stability limits of natural gas diffusion flames with swirl". *Eighteenth Symposium (International) on Combustion,* ***18***(1), pp. 667 – 677.

[9] Mongia, H. C., 2011. "Engineering aspects of complex gas turbine combustion mixers part IV: Swirl cup". *AIAA Paper 2011*.

[10] Fanaca, D., Alemela, P. R., Hirsch, C., and Sattelmayer, T., 2010. "Comparison of the flow field of a swirl stabilized premixed burner in an annular and a single burner combustion chamber". *Journal of Engineering for Gas Turbines and Power,* ***132***, 04.

[11] Guiberti, T., Durox, D., Scouflaire, P., and Schuller, T., 2015. "Impact of heat loss and hydrogen enrichment on the shape of confined swirling flames". *Proceedings of the Combustion Institute,* ***35***, pp. 1385 – 1392.

[12] Chong, L. T. W., Komarek, T., Zellhuber, M., Lenz, J., Hirsch, C., and Polifke, W., 2009. "Influence of strain and heat loss on flame stabilization in a non-adiabatic combustor". In proceedings of the 4th European Combustion Meeting, Vienna, April 14-17, 2009.

[13] Gupta A. K., Lilley D. G., S. N., 1984. *Swirl flows*. Abacus Press, Tunbridge Wells, Kent, England.

[14] Chterev, I., Sundararajan, G., Seitzman, J., and Lieuwen,

T., 2015. “Precession effects on the relationship between time-averaged and instantaneous swirl flow and flame characteristics”. In ASME Paper GT2015-42768.

[15] Toh, I., Honnery, D., and Soria, J., 2010. “Axial plus tangential entry swirling jet”. *Experiments in Fluids,* ***48***, pp. 309–325.

[16] Burmberger, S., Hirsch, C., and Sattelmayer, T., 2006. “Designing a radial swirler vortex breakdown burner”. In ASME Paper GT2006-90497.

[17] Burmberger, S., Hirsch, C., and Sattelmayer, T., 2006. “Design rules for the velocity field of vortex breakdown swirl burners”. In ASME Paper GT2006-90495.

[18] Syred, N., and Beér, J., 1974. “Combustion in swirling flows: A review”. *Combustion and Flame,* ***23***, pp. 143 – 201.

[19] Al-Abdeli, Y. M., and Masri, A. R., 2015. “Review of laboratory swirl burners and experiments for model validation”. *Experimental Thermal and Fluid Science,* ***69***, pp. 178 – 196.

[20] Durox, D., Moeck, J. P., Bourgouin, J.-F., Morenton, P., Viallon, M., Schuller, T., and Candel, S., 2013. “Flame dynamics of a variable swirl number system and instability control”. *Combustion and Flame,* ***160***, pp. 1729 – 1742.

[21] Claypole, T., and Syred, N., 1981. “The effect of swirl burner aerodynamics on NOx formation”. *Eighteenth Symposium (International) on Combustion,* ***18***(1), pp. 81 – 89.

[22] Sheen, H., Chen, W., Jeng, S., and Huang, T., 1996. “Correlation of swirl number for a radial-type swirl generator”. *Experimental Thermal and Fluid Science,* ***12***(4), pp. 444 – 451.

[23] Holäpfel, F., Lene, B., and Leuckel, W., 1996. “Swirl-induced intermittency: A novel effect modifying the turbulence structure of swirling free jets”. *Symposium (International) on Combustion,* ***26***(1), pp. 187 – 194.

[24] Kalt, P. A., Al-Abdell, Y. M., Masri, A. R., and Barlow, R. S., 2002. “Swirling turbulent non-premixed flames of methane: Flow field and compositional structure”. *Proceedings of the Combustion Institute,* ***29***(2), pp. 1913 – 1919.

[25] Jourdaine, P., Mirat, C., Beaunier, J., Caudal, J., Joumani, Y., and Schuller, T., 2016. “Effect of quarl on N2- and CO2-diluted methane oxy-flames stabilized by an axial-plus-tangential swirler”. In ASME Paper GT2016-56953.

[26] Darabiha, N., 1992. “Transient behaviour of laminar counterflow hydrogen-air diffusion flames with complex chemistry”. *Combustion Science and Technology,* ***86***, pp. 163–181.

[27] Docquier, N., and Candel, S., 2002. “Combustion control and sensors: a review”. *Progress in Energy and Combustion Science,* ***28***, pp. 107 – 150.

[28] Glassman, I., and Yetter, R. A., 2008. *Combustion (Fourth Edition)*, fourth edition ed. Academic Press.

[29] Eckbreth, A., 1996. *Laser Diagnostics for Combustion Temperature and Species*. Gordon & Breach.

[30] Hassel, E. P., and Linow, S., 2000. “Laser diagnostics for studies of turbulent combustion”. *Measurement Science and Technology,* ***11***(2), p. R37.

[31] Hartung, G., Hult, J., Kaminski, C. F., Rogerson, J. W., and Swaminathan, N., 2008. “Effect of heat release on turbulence and scalar-turbulence interaction in premixed combustion”. *Physics of Fluids,* ***20***(3).

[32] Lam, K., Davidson, D. F., and Hanson, R. K., 2013. “A shock tube study of H2 + OH $\rightarrow$ H2O + H using OH laser absorption”. *International Journal of Chemical Kinetics,* ***45***(6), 6, pp. 363–373.

[33] Durox, D., Ducruix, S., and Lacas, F., 1999. “Flow seeding with an air nebulizer”. *Experiments in Fluids,* ***27***, pp. 408–413.

[34] Kim, K. T., Lee, J. G., Lee, H. J., Quay, B. D., and Santavicca, D. A., 2010. “Characterization of forced flame response of swirl-stabilized turbulent lean-premixed flames in a gas turbine combustor”. *Journal of Engineering for Gas Turbines and Power,* ***132***.

[35] Ghoniem, A. F., and Knio, O. M., 1988. “Numerical simulation of flame propagation in constant volume chambers”. *Symposium (International) on Combustion,* ***21***, pp. 1313 – 1320.

[36] Schneider, C., Dreizler, A., and Janicka, J., 2005. “Fluid dynamical analysis of atmospheric reacting and isothermal swirling flows”. *Flow, Turbulence and Combustion,* ***74***(1), pp. 103–127.

[37] Guiberti, T. F., Durox, D., Zimmer, L., and Schuller, T., 2015. “Analysis of topology transitions of swirl flames interacting with the combustor side wall”. *Combustion and Flame,* ***162***(11), pp. 4342 – 4357.